

Probability Bounds Analysis for Nonlinear Population Ecology Models

Joshua A. Enszer¹, D. Andrei Măceș, Mark A. Stadtherr²

*Department of Chemical and Biomolecular Engineering,
University of Notre Dame, Notre Dame, IN 46556, USA*

Abstract

Mathematical models in population ecology often involve parameters that are empirically determined and inherently uncertain, with probability distributions for the uncertainties not known precisely. Propagating such imprecise uncertainties rigorously through a model to determine their effect on model outputs can be a challenging problem. We illustrate here a method for the direct propagation of uncertainties represented by probability bounds through nonlinear, continuous-time, dynamic models in population ecology. This makes it possible to determine rigorous bounds on the probability that some specified outcome for a population is achieved, which can be a core problem in ecosystem modeling for risk assessment and management. Results can be obtained at a computational cost that is considerably less than that required by statistical sampling methods such as Monte Carlo analysis. The method is demonstrated using three example systems, with focus on a model of an experimental aquatic food web subject to the effects of contamination by ionic liquids, a new class of potentially important industrial chemicals.

Keywords: Parameter uncertainty, Probability distributions, Population ecology, Food webs, Nonlinear dynamics, Ionic liquids

1. Introduction

Mathematical models are often the only resource available to predict the effects of anthropogenic influence on ecological systems. Limited physical experiments can possibly isolate and estimate the interactions between a subset of species in an ecosystem, or determine the effects of a change to the environment (e.g., a change in some resource or the introduction of a new resource, predator, or contaminant). However, it is difficult to replicate many such interactions or changes with physical experiments.

It can also be challenging to develop and effectively use mathematical models of ecosystems, particularly in the presence of uncertainty. The importance of dealing with the many potential sources of uncertainty in developing and using population ecology models is well known [e.g., 1–4]. Our focus here is on those types of uncertainty (e.g., measurement error, natural variation) that may manifest themselves as uncertainties in model parameters. Given some quantitative description of the parameter uncertainty, such as an interval or a probability distribution, the general goal of uncertainty analysis is to quantify the effect of such uncertainty on the model

outputs, or, in other words, to “propagate” the parameter uncertainty to the outputs. For relatively simple static or algebraic models, this might be done directly, perhaps using interval arithmetic or appropriate convolutions of probability distributions. For more complex or dynamic models, this is widely done using various sampling methods (e.g., Monte Carlo) in which model outputs are computed repeatedly at many different samples of the parameter values, with samples taken based on a specified probability distribution, if available.

In the presence of multiple types of uncertainty, it may be appropriate to describe the parameter uncertainty using probability bounds [3, 5, 6]. In this case, probability distributions are not known precisely but instead bounds on the cumulative probability distributions are given, thus effectively combining the ideas of intervals and probability distributions. For example, probability bounds may be a useful treatment of uncertainty when both measurement error (often represented by “error bars”, i.e., intervals) and natural variability (often represented by probability distributions) are present. When probability bounds are used, direct propagation of the uncertainty is again possible for reasonably simple static or algebraic models, and there is software available for this purpose [6]. For more complex or dynamic models, sampling methods can again be used; however, this is now a second-order (or two-dimensional) process [7], in which first a sample of the probability distribution for the parameters is taken from within their given probabil-

Email address: markst@nd.edu (Mark A. Stadtherr)

¹Current address: Department of Chemical and Biomolecular Engineering, University of Delaware, Newark, DE 19716 USA

²Corresponding author

ity bounds, and then this probability distribution is used to sample the parameter values. Such a nested sampling procedure can become quite expensive computationally.

We illustrate here a method for the direct propagation of uncertainties represented by probability bounds through nonlinear, continuous-time, dynamic models in population ecology. Uncertainties represented by simple intervals or probability distributions can also be handled, as special cases, using this approach. No sampling is required, and computed bounds on outputs are mathematically and computationally rigorous. This approach was originally developed [8] for applications in chemical process reaction engineering.

This paper is organized as follows. In the next section, we will provide some brief background on the key mathematical tools used, in particular intervals, and their extension to probability boxes, and Taylor models. Then we will provide a concise mathematical statement of the general problem to be solved, followed by a summary of the solution methods used. We will then demonstrate these methods using three example systems, with focus on a model of an experimental aquatic food web subject to the effects of chemical contamination.

2. Background

2.1. Interval Analysis

One simple way of representing uncertainty in a model parameter is to treat it as an interval. This is appropriate if upper and lower bounds are known, but there is no information about a probability distribution. Formally, we define a real interval X as the set of real numbers between (and including) a specified lower bound (denoted by \underline{X}) and upper bound (denoted by \overline{X}). That is, $X = [\underline{X}, \overline{X}] = \{x \in \mathbb{R} \mid \underline{X} \leq x \leq \overline{X}\}$. A real interval vector $\mathbf{X} = (X_1, X_2, \dots, X_n)^T$ has n real intervals as components and can be regarded as an n -dimensional rectangle or box. Interval matrices are similarly defined. Arithmetic on intervals is defined according to $X \text{ op } Y = \{x \text{ op } y \mid x \in X, y \in Y\}$, $\text{op} \in \{+, -, \times, \div\}$. Division in the case of $0 \in Y$ is allowed only in extensions of interval arithmetic [9]. Interval versions of the elementary functions can be similarly defined. Interval computations are implemented with outward rounding (lower bound rounded down, upper bound rounded up). Thus, interval computations can be used to obtain rigorously guaranteed bounds on function ranges, and play a key role in the verified (or validated) numerical solution of a variety of problems in science and engineering [10].

For a real function $f(x)$ of n variables, the interval extension $F(\mathbf{X})$ provides bounds on the range of $f(x)$ for $x \in \mathbf{X}$. That is, $\{f(x) \mid x \in \mathbf{X}\} \subseteq F(\mathbf{X})$. However, while these bounds are guaranteed, they are not necessarily tight. If $F(\mathbf{X})$ is computed using interval arithmetic (by replacing x with \mathbf{X} in the expression for $f(x)$), and if any variable occurs more than once in this expression, then the function range may be overestimated

due to the “dependency” problem. This occurs because, in interval arithmetic, separate occurrences of the same variable are not recognized as dependent. Another potential source of overestimation (lower bounds too low, upper bounds too high) in the use of interval methods is the “wrapping” effect [11]. This occurs when a multidimensional interval is used to enclose (wrap) a set of results that is not an interval. If this type of overestimation is propagated, say from step to step in an integration method for ordinary differential equations (ODEs), it can lead quickly to the loss of a meaningful enclosure. Historically, the issues of wrapping and dependency have resulted in interval methods acquiring a reputation for producing overly loose and conservative bounds. However, current interval methods, including the use of techniques such as Taylor models, as discussed below, can often yield rigorous bounds with very little overestimation. Several good introductions to interval analysis, as well as interval arithmetic and other aspects of computing with intervals, are available [9, 10, 12–15].

2.2. Probability Boxes (P-Boxes)

An interval gives an upper and lower bound only, and provides no knowledge about the distribution of uncertainties. If some (but not exact) knowledge about the distribution is available, then this can be captured by using “probability boxes” (p-boxes), which provide interval-like bounds on the cumulative distribution function (CDF) [6, 8, 16, 17]. Intervals and exact CDFs represent special cases of the more general concept of the p-box.

For some quantity (variable or parameter) x , we define the CDF $F_x(z)$ as giving the probability that $x \leq z$. A p-box for x , denoted $\text{PB}(x) = (L_x, R_x)$, is the set of all such CDFs enclosed by two bounding CDFs $L_x(z)$ and $R_x(z)$ with finite support. That is, $\text{PB}(x) = (L_x, R_x) = \{F_x(z) \mid L_x(z) \geq F_x(z) \geq R_x(z)\}$. For a given value of z , the left bounding function $L_x(z)$ of the p-box gives the upper bound on the probability that $x \leq z$ and the right bounding function $R_x(z)$ gives the lower bound on this probability. This is shown for an example p-box in Fig. 1(a), which is marked to indicate that, for this p-box, the probability that $x \leq 2$ is bounded by the interval $[0.4, 0.6]$. Conversely, for a given value of the cumulative probability, $L_x(z)$ and $R_x(z)$ provide lower and upper bounds on the values of x for which this probability is possible. For the case of the p-box in Fig. 1(b), this shows that the 40th percentile value of x is bounded by the interval $[1.78, 2]$. The bounding functions in Fig. 1 are (truncated) Gaussian CDFs. However, the p-box encloses both Gaussian and non-Gaussian CDFs.

Williamson and Downs [5] have presented methods for rigorously bounding the results of arithmetic (or other) operations on random variables when only their bounding distributions are known. This can be done without assuming any information about possible correlation between the operands. It can also be done for

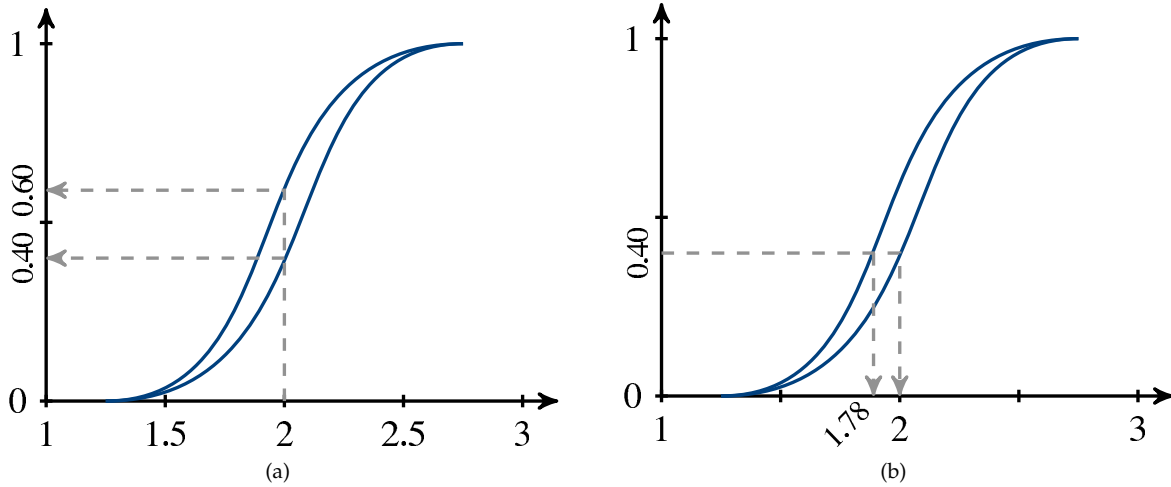


Figure 1: Interpretation of a p-box $PB(x)$: (a) The probability that $x \leq 2$ is bounded by the interval $[0.40, 0.60]$. (b) The 40th percentile value of x is bounded by the interval $[1.78, 2.00]$.

the cases that the operands are independent, or that they are the same, such as in a polynomial or other expression with a repeated operand. In general, these methods are implemented numerically, and use piecewise-constant discretizations of the bounding distributions. For the discretization, the p-box bounds are enclosed using an ordered set of d intervals, each representing a probability range of equal weight $1/d$. Subsequent operations are then done on these intervals using interval arithmetic. A detailed example of an arithmetic operation on two p-boxes is given by Enszer et al. [8], who also demonstrate how the dependency and wrapping issues extend from interval operations to p-box operations. Analogous procedures can be used to determine probability bounds on the results of other functions (e.g., logarithm, integral powers, polynomial, etc.) Obviously, a tighter enclosure of a p-box can be obtained using a finer discretization. Unless noted otherwise, all of the computations done in the examples presented here use $d = 100$ intervals to discretize a p-box.

P-box operations are implemented in the risk analysis software RAMAS Risk Calc [6], and basic p-box arithmetic operations may also be done using Statool [18]. Neither of these software platforms perform verified computations with outward rounding. For this purpose, we have developed a small library of functions for p-box generation and arithmetic for use with MATLAB, including the option to implement directed outward rounding. This is the tool that is used for the p-box computations in the examples presented below.

2.3. Taylor Models

One approach for addressing the issues of dependency and wrapping that may lead to overestimation of bounds in traditional interval methods is the use of Taylor models [19, 20]. In this approach, a function is represented over some desired interval by a ‘‘Taylor model,’’

which consists of a real-valued Taylor polynomial and an interval-valued remainder bound. The basic idea follows directly from the Taylor theorem. For a real function $f(x)$ that is $(q + 1)$ times partially differentiable on the interval X and $x_0 \in X$, the Taylor theorem says that for each $x \in X$, there exists a real ζ with $0 < \zeta < 1$ such that

$$f(x) = p_f(x - x_0) + r_f(x - x_0, \zeta), \quad (1)$$

where p_f is a q -th order real-valued polynomial (truncated Taylor series) in $(x - x_0)$ and r_f is a remainder, which can be bounded quantitatively over $0 < \zeta < 1$ and $x \in X$ using interval arithmetic or other methods to obtain an interval-valued remainder bound R_f . A q -th order Taylor model $T_f = p_f + R_f$ for $f(x)$ over X then consists of the polynomial p_f and the remainder bound R_f and is also denoted by $T_f = (p_f, R_f)$. Note that, according to the Taylor theorem, $f(x) \in T_f$ for $x \in X$, and thus we have the key property that T_f encloses the range of $f(x)$ over X .

In practice, Taylor models of functions are often computed by performing Taylor model operations. Arithmetic with Taylor models can be done using the operations described by Makino and Berz [19, 20, 21], which include addition, multiplication, reciprocal, and intrinsic functions. In this way, it is possible to start with simple functions such as the constant function $f(x) = k$, for which $T_f = (k, [0, 0])$, and the identity function $f(x_i) = x_i$, for which $T_f = (x_{i0} + (x_i - x_{i0}), [0, 0])$, and to then compute Taylor models for quite complicated functions. Implementations based on operator overloading make it easy to compute a Taylor model for any function that can be computed using standard arithmetic operations and elementary functions. Compared to other rigorous bounding techniques, the Taylor model approach often yields tighter bounds for modest to complicated functional dependencies [19, 20, 22]. The use of Taylor

models for function bounding does not eliminate the dependency problem; however, by capturing all the dependencies in a single polynomial, a functional form which can generally be bounded fairly tightly, especially over relatively small intervals, the effect of dependencies can be greatly suppressed.

3. Problem Statement

In this section, we describe the basic problem to be addressed, and describe our goals for its solution. Consider an initial value problem (IVP) for a parametric, autonomous system of ODEs with uncertain parameters and initial states:

$$\frac{d\mathbf{y}}{dt} = \mathbf{f}(\mathbf{y}, \boldsymbol{\theta}), \quad \mathbf{y}(t_0) = \mathbf{y}_0 \in \mathbf{Y}_0, \quad \boldsymbol{\theta} \in \boldsymbol{\Theta}. \quad (2)$$

Here \mathbf{y} is the vector (length n) of state variables with initial value \mathbf{y}_0 , $\boldsymbol{\theta}$ is a vector (length p) of time-invariant parameters, and $t \in [t_0, t_f]$ for some $t_f > t_0$. \mathbf{Y}_0 and $\boldsymbol{\Theta}$ are interval vectors that enclose uncertainties in the initial states and parameters, respectively. It is assumed that some information about the probability distribution of the uncertainty is available for one or more component of \mathbf{Y}_0 or $\boldsymbol{\Theta}$, and that this can be expressed as a p-box, as defined above in Section 2.2. It is also assumed that \mathbf{f} is representable by a finite number of standard functions, and that \mathbf{f} is $(k - 1)$ times continuously differentiable with respect to \mathbf{y} and $(q + 1)$ times continuously differentiable with respect to $\boldsymbol{\theta}$. Here, k is the order of the truncation error in the interval Taylor series (ITS) method used in the solution procedure outlined below, and q is the order of the Taylor model used to represent dependence on parameters and initial values. For ODE models that are nonautonomous, or that have parameters with known time dependence, conversion to the form of Eq. (2) can be achieved by the introduction of additional state variables.

There are two goals: 1. Because of the uncertainty in the parameters and initial states, there is a range of possible solutions $\mathbf{y}(t)$ to Eq. (2). Our first goal is to determine rigorous (mathematically guaranteed) upper and lower bounds on this range of state trajectories. To do this, we will determine enclosures \mathbf{Y}_j of the state variables $\mathbf{y}_j = \mathbf{y}(t_j)$ at the endpoints $t_j \in [t_0, t_f]$ of every time step in the numerical integration method used to solve Eq. (2). 2. Because the probability distribution of the uncertainties is itself uncertain, the probabilities that particular state values will be observed at a given time is also uncertain. Our second goal, which is of particular interest here, is to determine rigorous (mathematically guaranteed) upper and lower bounds on these uncertain probabilities. To do this we will determine, for any enclosure $\mathbf{Y}_j \ni \mathbf{y}_j$, verified bounds, in the form of a p-box, on the probability distribution for the values of \mathbf{y}_j . Thus, rigorous bounds are obtained on the probabilities that different states are achieved.

4. Solution Procedure

4.1. Enclosure of State Variables

For addressing the first goal stated in Section 3, a number of approaches have been proposed, including defect-based methods [23] and methods based on differential inequalities [24, 25]. However, most work has focused on the use of interval methods (also called validated methods or verified methods). These are generally based on a two-phase process employed at each integration step. In the first phase, existence and uniqueness of the solution are proven, and a rough enclosure of the solution is determined. In the second phase, a tighter enclosure of the solution is computed. In general, both phases may be implemented using interval Taylor series (ITS) expansions with respect to time, with use of automatic differentiation to obtain the Taylor coefficients. An excellent review of traditional interval methods for ODEs has been given by Nedialkov et al. [26], and more recent work has been reviewed by Neher et al. [27]. To address this problem, there are several packages available, involving a variety of different methods; these packages include VNODE [26, 28], VNODE-LP [29], COSY VI [30], RiOT [31], ValEncIA-IVP [23], and VSPODE [32]. We will make use here of VSPODE, which employs a novel type of Taylor model, based on use of a parallelepiped (instead of interval) remainder bound, to deal with the dependency and wrapping issues arising from the uncertain parameters and initial values.

The fundamental idea in Taylor model methods, as used in VSPODE, is to determine an *explicit analytical expression* for the state variables, at any given time, in terms of the initial states and the problem parameters. This analytical expression is in the form of a Taylor model, which can then be bounded over the specified range and probability distribution of initial state and parameter values. In particular, assuming an interval enclosure \mathbf{Y}_j of the state variables at time t_j , an integration step in VSPODE determines a time step $h_j = t_{j+1} - t_j$ and an enclosure \mathbf{Y}_{j+1} of the state variables at t_{j+1} . The time step used can be specified, but will be reduced if necessary, in the first phase of VSPODE, to guarantee existence of a unique solution $\mathbf{y}(t)$ for $t \in [t_j, t_{j+1}]$ and for all $\mathbf{y}_j \in \mathbf{Y}_j$ and all $\boldsymbol{\theta} \in \boldsymbol{\Theta}$. In the second phase of VSPODE, a Taylor model $\mathbf{T}_{\mathbf{y}_{j+1}}(\mathbf{y}_0, \boldsymbol{\theta})$, of \mathbf{y}_{j+1} in terms of the parameters $\boldsymbol{\theta}$ and initial states \mathbf{y}_0 , is determined. This is an explicit analytical expression for $\mathbf{y}_{j+1} = \mathbf{y}(t_{j+1})$ in terms of the initial states \mathbf{y}_0 and parameters $\boldsymbol{\theta}$, which is valid for all $\mathbf{y}_0 \in \mathbf{Y}_0$ and all $\boldsymbol{\theta} \in \boldsymbol{\Theta}$. The interval state bounds \mathbf{Y}_{j+1} can now be determined by bounding $\mathbf{T}_{\mathbf{y}_{j+1}}(\mathbf{y}_0, \boldsymbol{\theta})$ over $\mathbf{y}_0 \in \mathbf{Y}_0$ and $\boldsymbol{\theta} \in \boldsymbol{\Theta}$ using interval arithmetic or other rigorous bounding methods. Complete details of the method outlined briefly here are given by Lin and Stadtherr [32]. Other interesting ideas for using Taylor models in state bounding have also been described recently [33, 34].

4.2. Probability Distribution of State Variables

The second goal is, given p-box bounds on the distributions of the uncertain quantities, to determine rigorous p-box bounds on the distributions for the values of the state variables $\mathbf{y}_j \in \mathbf{Y}_j$.

Using the procedure described above, one can obtain, for a particular time t_j of interest, a Taylor model $T_{y_j}(\mathbf{y}_0, \boldsymbol{\theta})$ giving the state variables $\mathbf{y}_j = \mathbf{y}(t_j)$ as a polynomial function of the initial states $\mathbf{y}_0 \in \mathbf{Y}_0$ and parameters $\boldsymbol{\theta} \in \boldsymbol{\Theta}$, plus a small remainder bound. The available p-boxes for \mathbf{y}_0 and for $\boldsymbol{\theta}$ are then substituted directly into $T_{y_j}(\mathbf{y}_0, \boldsymbol{\theta})$, and a p-box providing bounds on the probability distribution for \mathbf{y}_j can be calculated using p-box operations. Note that the Taylor model now has p-box, rather than real number, operands. The direct application of p-box arithmetic operations in evaluating the Taylor model may lead to significant overestimation of bounds on the true probability distribution of the state variables, due to the wrapping and dependency problems of p-box arithmetic discussed previously. This occurs in part because, in using p-box arithmetic operations, the polynomial structure of the Taylor model, which tends to suppress dependency issues, is not being effectively exploited. Thus special care is needed to obtain tighter bounds.

One straightforward approach, which can result in a considerably tighter enclosure, is to treat the Taylor model $T_{y_j}(\mathbf{y}_0, \boldsymbol{\theta})$ as a single "operation" or standard function, rather than as a collection of individual multiplication and addition operations involving the same operands. That is, p-boxes are not constructed after the individual operations, each of which may result in some overestimation due to wrapping and dependency, but instead are only constructed after bounding of the entire Taylor model function. This approach, which we refer to as "discrete interval bounding" (DIB) effectively transforms the p-box computation into a series of Taylor model bounding computations, each over different subintervals of \mathbf{Y}_0 and $\boldsymbol{\Theta}$. The bounding can be done with interval arithmetic, or using some other approach for bounding polynomials. For example, VSPODE bounds the Taylor model polynomials by first considering the constant, linear and diagonal quadratic terms, the sum of which can be bounded exactly [32]. The remaining off-diagonal quadratic and higher-order terms are then bounded using interval arithmetic.

An effective complement to the DIB approach is subinterval reconstitution (SIR) [17]. In SIR, each of the d discretization intervals used for p-box operations is further partitioned into d_s subintervals. Operations are then done on each subinterval separately, and the overall results for a particular discretization interval are reconstituted by taking the union of the results from each of its subintervals. SIR is available as an option in RAMAS Risk Calc, as well as in our MATLAB library of functions for p-box computation. SIR and DIB are most useful for

cases, as encountered here in the Taylor model polynomial, in which there are repeated occurrences of variables in the expression to be evaluated.

A package of codes (C++ and MATLAB) implementing the methods described here, together with the files needed to run the example problems described below, is available for noncommercial use from the corresponding author.

5. Examples

In this section, we apply the techniques described above to a set of examples. Each example involves a nonlinear population dynamics model that has parameters and/or initial conditions which are uncertain, and which have imprecise probability distributions represented by p-boxes. In all examples, we will assume that the uncertain quantities are independent (uncorrelated). Since our solution procedures are designed to be general-purpose, we will not attempt to exploit any special properties in the example problems.

VSPODE was implemented using its default ITS truncation order ($k = 17$) and Taylor model order ($q = 5$). All the example problems were solved on a dual-core AMD Opteron™ Model 1214 processor (2.2 GHz) running Ubuntu 11.04. VSPODE was implemented using C++. P-box arithmetic was implemented using MATLAB, with outward rounding of interval operations done using techniques described by Lambov [35] that do not require repeated switching of rounding mode. Second-order Monte Carlo simulations used as comparisons were also implemented using MATLAB.

5.1. Lotka-Volterra Competition Model

As an illustrative example, we will consider the Lotka-Volterra model of competition. In this model, two species grow logistically, but each competes for a portion of the resources (carrying capacity) needed by the other. The model can be written as

$$\begin{aligned} \frac{dx_1}{dt} &= r_1 x_1 \left[1 - \frac{x_1 + \alpha_{12} x_2}{K_1} \right] \\ \frac{dx_2}{dt} &= r_2 x_2 \left[1 - \frac{x_2 + \alpha_{21} x_1}{K_2} \right]. \end{aligned} \quad (3)$$

Here x_1 and x_2 are the populations of the two competing species, r_1 and r_2 are their intrinsic growth rates per capita, and K_1 and K_2 are their carrying capacities. The nature of the competition is governed by the interaction parameters α_{12} , representing the impact of species 2 on species 1, and α_{21} , representing the impact of species 1 on species 2.

For this example, we will first consider the case in which the model parameters are known, but the initial populations are uncertain. Values of the model parameters are $r_1 = 1.0$, $r_2 = 0.6$, $K_1 = 560$, $K_2 = 202$, $\alpha_{12} = 2.66$

and $a_{21} = 0.31$. Values of the initial populations, $x_{1,0}$ and $x_{2,0}$ are assumed to vary no more than 10% from mean values of 150 and 130. That is, $x_{1,0} \in [135, 165]$ and $x_{2,0} \in [117, 143]$. Furthermore, we assume that the CDFs for $x_{1,0}$ and $x_{2,0}$ are bounded by the p-boxes shown in Fig. 2. This p-box assumes uniform bounding distributions from a lower bound that is 8 to 10% below the mean to an upper bound that is 8 to 10% above the mean. The time horizon of interest is $t \in [0, 150]$.

Using VSPODE, we determined rigorous enclosures for the trajectories $x_1(t)$ and $x_2(t)$ over the desired time horizon. These are shown by the solid black curves in Fig. 3, which provide upper and lower bounds on the state trajectories. To test the tightness of these bounds, we compared them to the results of a simple Monte Carlo simulation with 500 trials. In each trial, values of $x_{1,0}$ and $x_{2,0}$ were sampled at random from within their given interval bounds, and the system was integrated using the ode45 ODE solver in MATLAB. The results of each trial is plotted in grey in Fig. 3, resulting in the mostly grey shaded area between the bounds computed by VSPODE. Bounds obtained from Monte Carlo analysis will yield an underestimate (inner estimate) of the true bounds (assuming that the ODE solver used in each trial correctly integrates the system, which typically cannot be guaranteed), and bounds obtained from VSPODE will yield an overestimate (outer estimate) of the true bounds, and are guaranteed to be correct. The results in Fig. 3 indicate that the VSPODE bounds are in fact very tight enclosures of the trajectories.

We now consider the probability distribution of state values at a specified time, say at $t = 4$ (near the peak possible value of x_1). Perhaps a question of interest is to determine the probability that x_1 does not exceed 170 at this time. To do this we use the Taylor model already computed by VSPODE for $t = 4$, together with the given p-boxes for $x_{1,0}$ and $x_{2,0}$, to compute p-boxes for $x_1(4)$ and $x_2(4)$, using the SIR and DIB procedures described above. The resulting p-boxes $PB(x_1(4))$ and $PB(x_2(4))$ are shown by the solid blue lines in Fig. 4. This shows that the probability of $x_1 \leq 170$ is in the interval [36, 47] %.

For comparison, we also performed a second-order Monte Carlo analysis to get probability distributions for $x_1(4)$ and $x_2(4)$. This procedure involves two nested loops of sampling. In the outer loop, CDFs for $x_{1,0}$ and $x_{2,0}$ were chosen at random from the set enclosed by $PB(x_{1,0})$ and $PB(x_{2,0})$ (for simplicity, only uniform distributions were chosen). Then, in the inner loop, the intervals of uncertainty for $x_{1,0}$ and $x_{2,0}$ were repeatedly sampled based on the CDFs chosen in the outer loop, and for each sample the ODE system was integrated. These results were then used to determine CDFs for $x_1(4)$ and $x_2(4)$. This process was then repeated for multiple outer loop samples of $PB(x_{1,0})$ and $PB(x_{2,0})$. Fig. 4 shows (red curves) CDFs from 100 outer loop samples, each obtained using 500 inner loop samples, together with the

p-boxes computed from the VSPODE Taylor model (blue curves) for comparison. The CPU time for obtaining the latter was 13 seconds, while the CPU time for the former (second-order Monte Carlo procedure) was 380 seconds. The p-boxes $PB(x_1(4))$ and $PB(x_2(4))$ obtained using the VSPODE Taylor model approach are rigorous bounds on the CDFs for $x_1(4)$ and $x_2(4)$, respectively. However, close examination of Figure 4 reveals that a small number of the CDFs obtained using the sampling approach actually lie partly outside of these rigorous bounds. This highlights the fact that the CDFs obtained by sampling are not rigorous, as this would require, in principle, an infinite number of inner loop samples.

As a second case based on the Lotka-Volterra competition example, we will consider a situation in which the initial states are known, but some of the model parameters are uncertain. Now $x_{1,0} = 150$ and $x_{2,0} = 130$, but we assume that there is $\pm 10\%$ uncertainty in the previously given values of r_1 and r_2 (other parameter values remain fixed at their previous values). Thus $r_1 \in [0.9, 1.1]$, $r_2 \in [0.54, 0.66]$. Also, we assume that the CDFs for r_1 and r_2 are bounded by the p-boxes shown in Fig. 5, which again are based on uniform bounding distributions from a lower bound that is 8 to 10% below the mean to an upper bound that is 8 to 10% above the mean.

Again we used VSPODE to determine rigorous enclosures for the trajectories $x_1(t)$ and $x_2(t)$, as shown Fig. 6. Using the VSPODE Taylor model for $t = 4$, we also again determined $PB(x_1(4))$ and $PB(x_2(4))$, which are shown by the blue curves in Fig. 7. A comparison of these p-boxes with a sampling approach (second-order Monte Carlo, with 100 outer loop and 500 inner loop samples) is also shown in Fig. 7. The CPU time needed for the VSPODE approach was 12 seconds, while the sampling approach required 323 seconds. Again we note that the sampling procedure did not yield entirely rigorous results.

5.2. Lotka-Volterra Predator-Prey Model

As a second illustrative example, we will use the well-known Lotka-Volterra predator-prey model [36, 37]. This model simulates the populations of two trophic levels, predator and prey, in an ecosystem. The model can be written as

$$\begin{aligned} \frac{dx_1}{dt} &= r_1 x_1 - a_{12} x_1 x_2 \\ \frac{dx_2}{dt} &= -d_2 x_2 + a_{21} x_1 x_2. \end{aligned} \tag{4}$$

Here x_1 and x_2 represent populations of the prey and predator, respectively, r_1 is the intrinsic net growth rate per capita of the prey, d_2 is the intrinsic death rate per capita of the predator, and a_{12} and a_{21} are predator-prey interaction parameters. We will use a two-parameter form of this model in which $r_1 = a_{12} = \theta_1$ and $d_2 = a_{21} = \theta_2$. The initial conditions are known and given by

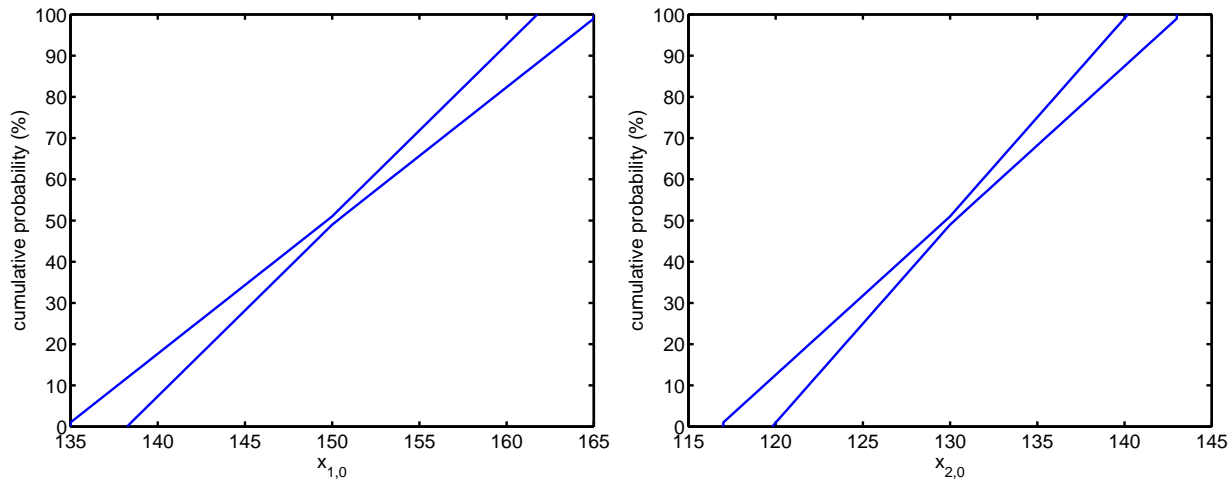


Figure 2: Assumed p-boxes for $x_{1,0}$ and $x_{2,0}$ for the Lotka-Volterra competition model (with uncertain initial conditions).

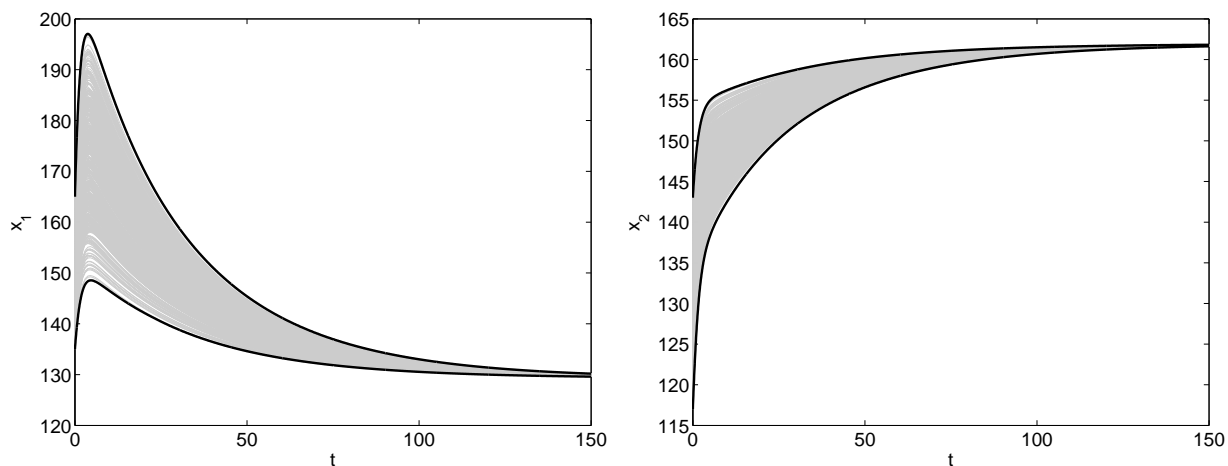


Figure 3: Trajectory bounds for x_1 and x_2 for the Lotka-Volterra competition model (with uncertain initial conditions) as computed by VSPODE are shown in black. The results of Monte Carlo simulation are shown in grey.

$x_{1,0} = 1.2$ and $x_{2,0} = 1.1$. The parameters are treated as uncertain with $\theta_1 \in [2.99, 3.01]$ and $\theta_2 \in [0.99, 1.01]$. For parameter values in these intervals, the trajectories will converge to stable limit cycles. The model in this form, and with these initial states and parameter values, is known to be difficult numerically, and is used in standard numerical test problems [38]. The CDFs for θ_1 and θ_2 are bounded by p-boxes that have uniform bounding distributions with fixed mean (at $\theta_1 = 3$ and $\theta_2 = 1$) and an uncertain standard deviation of $[0.005, 0.0057]$. The time horizon of interest is $t \in [0, 25]$.

Using VSPODE, we determined rigorous enclosures for the trajectories $x_1(t)$ and $x_2(t)$, as shown by the solid black curves in Fig. 8. These represent rigorous upper and lower bounds on the state trajectories. Fig. 8 also shows the results of a Monte Carlo simulation (500 samples) in grey. As in the previous example, we used the ode45 ODE solver in MATLAB in doing the Monte Carlo

analysis. However, when default tolerances were used in ode45, the computed trajectories did not fall within the rigorous VSPODE bounds, suggesting that the ode45 results were incorrect. By increasing the ode45 tolerances to a relative tolerance of 10^{-12} and an absolute tolerance of 10^{-14} it was possible to obtain results from ode45 that fall within the rigorous VSPODE trajectory bounds. While VSPODE has computed tight bounds for $t \in [0, 25]$, it is important to note that, for difficult problems such as this one, VSPODE will sometimes fail to determine meaningful bounds beyond some value of t [32]. For this problem, the breakdown of bounds occurs at about $t = 30$.

Using the Taylor models computed by VSPODE, we can now determine p-boxes for the prey and predator populations at times of interest. Results (blue bounding curves) are shown for $t = 10$ (Fig. 9), $t = 20$ (Fig. 10), and $t = 25$ (Fig. 11). As might be expected, the relative

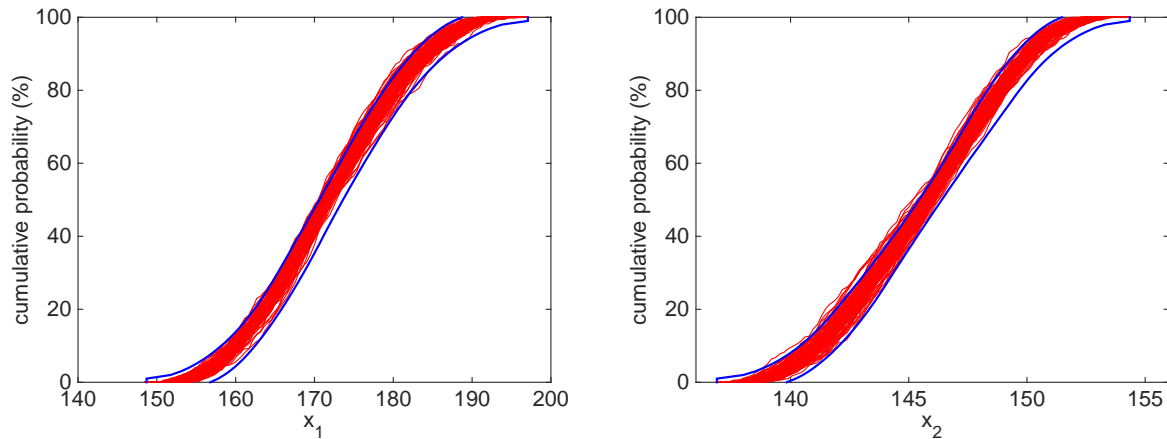


Figure 4: P-boxes (blue) computed from VSPODE Taylor models compared to second-order Monte Carlo simulation (red) for x_1 and x_2 at $t = 4$ for the Lotka-Volterra competition model (with uncertain initial conditions).

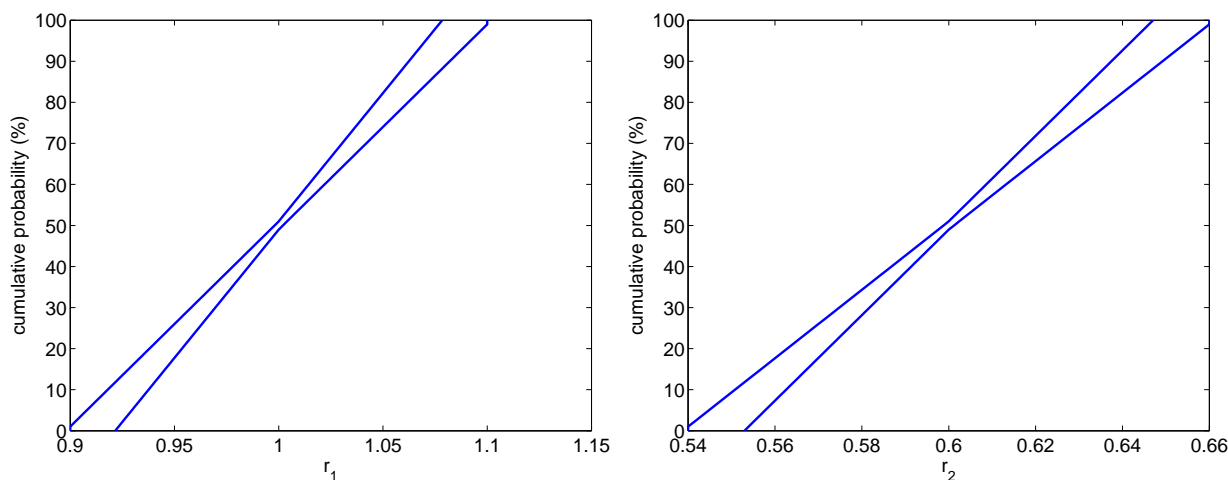


Figure 5: Probability enclosures for r_1 and r_2 for the Lotka-Volterra competition model (with uncertain growth rate parameters).

widths of the p-boxes increase with time, as there is increasing uncertainty in the trajectories as time increases (see Fig. 8). The shape of the p-boxes depends on the position in the limit cycle. For example, at $t = 10$ the predator population x_2 is near a minimum and slowly beginning to grow, while at $t = 20$ it is going through a fairly steep decline. This difference in rate of change is reflected in the relative steepness of $PB(x_2(10))$ (Fig. 9) and $PB(x_2(20))$ (Fig. 10). A similar effect can be seen for $PB(x_1(25))$ (Fig. 11), since at $t = 25$, the prey population x_1 is almost exactly at a maximum.

For comparison, we also did second-order Monte Carlo analysis, again with 100 outer loop and 500 inner loop samples, and these results are shown in red in Figs. 9-11. The average computation time for these three cases was 13 seconds for the direct (VSPODE) approach, and 38700 seconds for the sampling approach. The need to use tighter than default tolerances for ode45 in MATLAB contributed to the large computational expense required

for the sampling approach. As in the previous examples, the results of sampling with 500 inner loops did not produce entirely rigorous results. It can also be seen that at $t = 25$ (Fig. 11) the p-box results for x_1 do not provide tight bounds near the peak value. This occurs because the VSPODE trajectory bounds near this peak are also slightly loose at $t = 25$, as can be seen by close examination of Fig. 8. Ways to tighten these bounds will be discussed in Section 5.3.

5.3. Aquatic Food Web Model

Our interest in ecosystem modeling is motivated in part by its potential use in studying the impact of the industrial use of newly developed materials. Obviously it is desirable to take a proactive, not reactive, approach in examining the safety and environmental effects of using new materials, and modeling can enable the development of such forward-looking strategies. Of particular interest is the potential use of room-temperature ionic

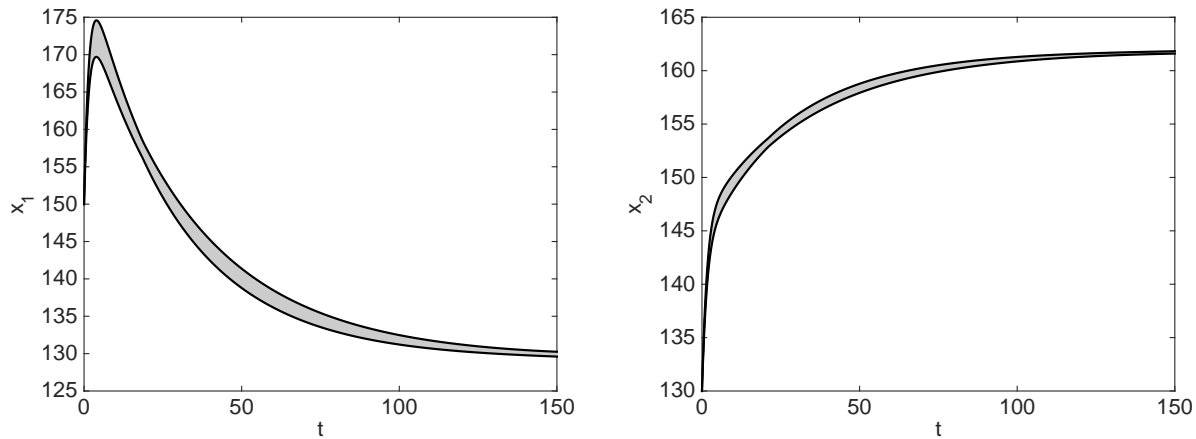


Figure 6: Trajectory bounds for x_1 and x_2 for the Lotka-Volterra competition model (with uncertain growth rate parameters) as computed by VSPODE. The results of Monte Carlo simulation are shown in grey.

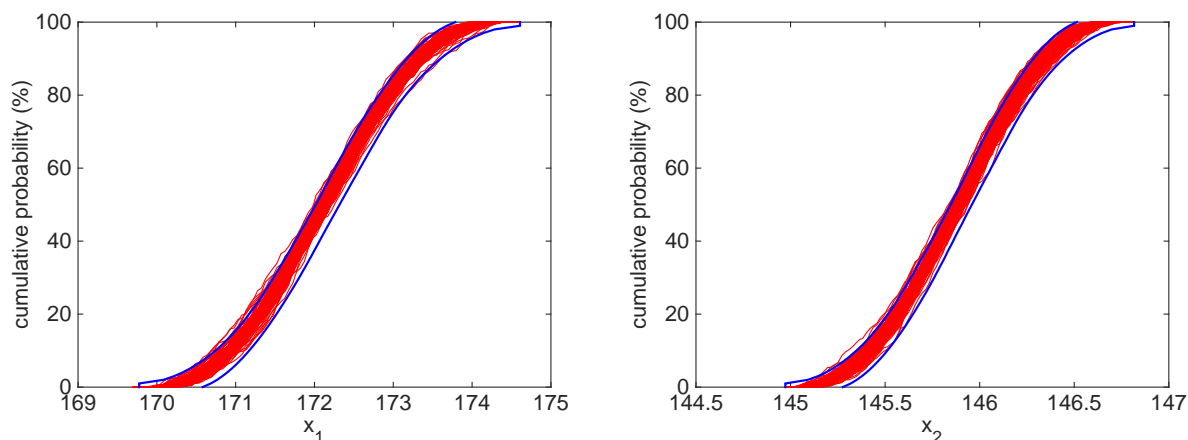


Figure 7: P-boxes (blue) computed from VSPODE Taylor models compared to second-order Monte Carlo simulation (red) for x_1 and x_2 at $t = 4$ for the Lotka-Volterra competition model (with uncertain growth rate parameters).

liquids (ILs) as “green” solvents in place of traditional solvents [39] and in a wide variety of applications, including CO₂ capture [e.g., 40, 41], low-GHG refrigeration [42], and many other energy-related fields [43].

ILs have exceedingly low vapor pressures (essentially they do not evaporate); thus, from a health, safety, and environmental standpoint, ILs offer several potential advantages when compared to the volatile organic compounds (VOCs) traditionally used as solvents. Such advantages include, for example, elimination of hazards due to flammability, explosion, inhalation, and air pollution. ILs are, however, soluble in water to varying degrees, so if ILs are used commercially on a large scale, their entry into aquatic ecosystems is of concern. Thus, in recent years there has been significant interest in studying the environmental fate and toxicity of ILs, as reviewed by Kulacki et al. [44], Pham et al. [45], and Bubalo et al. [46]. However, while some physical experiments on isolated simulations of an ecosystem are possible, these

are often expensive, time-consuming, or otherwise limited. As emphasized by Bubalo et al. [46], to estimate complex, multi-species effects on entire food chains, a modeling approach should be used since standard tests are inadequate.

The population model considered here was developed by Kulacki [47] for the study of multiple stressors (ILs, invasive species) on a simple freshwater lake community. In this model, the species monitored are the phytoplankton *Chlamydomonas reinhardtii* (C), the zooplankton *Daphnia magna* (D), and the zebra mussel *Dreissena polymorpha* (Z). The model equations are:

$$\begin{aligned}
 \frac{dC}{dt} &= C \left[r_C \left(1 - \frac{C}{K_C} \right) - \frac{a_{CD}D}{b_C + C} - a_{CZ}Z \right] \\
 \frac{dD}{dt} &= D \left[\frac{a_{DC}C}{b_C + C} \left(1 - \frac{D}{K_D} \right) - d_D \right] \\
 \frac{dZ}{dt} &= Z [a_{ZC}C - d_Z].
 \end{aligned} \tag{5}$$

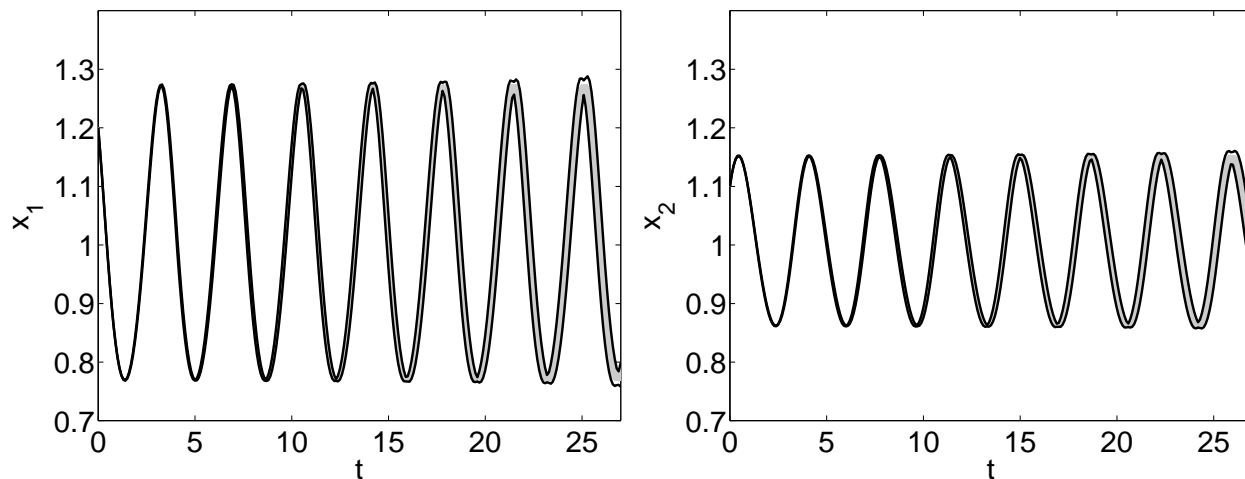


Figure 8: Trajectory bounds for x_1 and x_2 for the Lotka-Volterra predator-prey model as computed by VSPODE. The results of Monte Carlo simulation are shown in grey.

This assumes logistic growth of *C. reinhardtii*, predation by *D. magna* on *C. reinhardtii* with a hyperbolic predator response and predator-dependent efficiency, and predation by *D. polymorpha* on *C. reinhardtii* with a linear predator response. The model parameters are identified in Table 1, along with experimentally determined values [47–50] at different concentrations of the IL 1-butyl-3-methylimidazolium bromide ([bmim][Br]). The time horizon of interest is $t \in [0, 30]$ days.

Note that the parameters r_C and a_{CD} are treated here as uncertain. The width of the uncertainty corresponds to approximately ± 1 standard deviation. The initial conditions were determined [47] based on a typical Midwestern USA lake that has been invaded by zebra mussels, and are also given in Table 1. The uncertainties in r_C and a_{CD} have CDFs that are bounded by p-boxes. These p-boxes have uniform bounding distributions with a lower bound that is 8 to 10% below the mean and an upper bound that is 8 to 10% above the mean. These parameters depend on contaminant level (see Table 1).

Rigorous enclosures for the trajectories $C(t)$, $D(t)$ and $Z(t)$ were determined using VSPODE for each of the three IL concentration levels, as shown by the solid black curves in Figs. 12–14. As might be expected, since the uncertain parameters most directly affect the *C. reinhardtii* population, the trajectories for $C(t)$ show the most sensitivity to the uncertainties. The upper and lower bounds for $D(t)$ and $Z(t)$ are close together and cannot be readily distinguished on the scale of Figs. 12–14. The results of Monte Carlo simulation (500 samples using ode45 in MATLAB with default tolerances) are shown in grey in Figs. 12–14. For the case of no IL contaminant, the population of *C. reinhardtii* initially rises but then passes through a maximum and declines due to increasing predation from *D. magna*. Introduction of the contaminant increases d_D and decreases a_{DC} , which inhibits the growth of *D. magna*, thus eliminating the de-

cline in *C. reinhardtii*, which reaches its highest population at the highest contaminant level.

Comparing the VSPODE bounds and the Monte Carlo simulation results for the no contaminant case (Fig. 12) shows that in this case the VSPODE bounds are becoming increasingly loose with increasing t , and are beginning to break down as $t = 30$ is approached. One simple approach to obtaining tighter bounds from VSPODE is to partition the interval of uncertainty into subintervals and to then apply VSPODE within each subinterval. The results obtained for each subinterval are then combined to determine trajectory bounds over the entire interval of uncertainty. This means that each subinterval will be characterized by a different Taylor model to relate the state variables to the uncertain quantities. The fact that different Taylor models apply to different subintervals of uncertainty must be then be accounted for in applying the procedure described in Section 4.2 for computing p-boxes for the state variables. The breakdown of bounds determined by VSPODE at longer simulation times does not occur in all problems (it does not occur in the examples of Section 5.1 or in the 2 mg/L or 4 mg/L contaminant levels in this example), and when it does occur the VSPODE bounds may diverge from the exact bounds quite gradually in some cases and very rapidly in others. In our experience, the behavior of the computed bounds at longer simulation times is highly problem dependent and, unfortunately, difficult to predict.

We can now use the Taylor models determined using VSPODE to compute probability bounds for the state variables at specified times of interest. For example, say we are interested in the probability that the *C. reinhardtii* population does not exceed 4×10^{17} at $t = 15$ days for the different contaminant levels. To address this question, the p-boxes for $C(15)$ at each contaminant level were determined, as shown in Fig. 15. For no contaminant, it is clear from Fig. 15a (and also from Fig. 12a) that $C(15)$ is

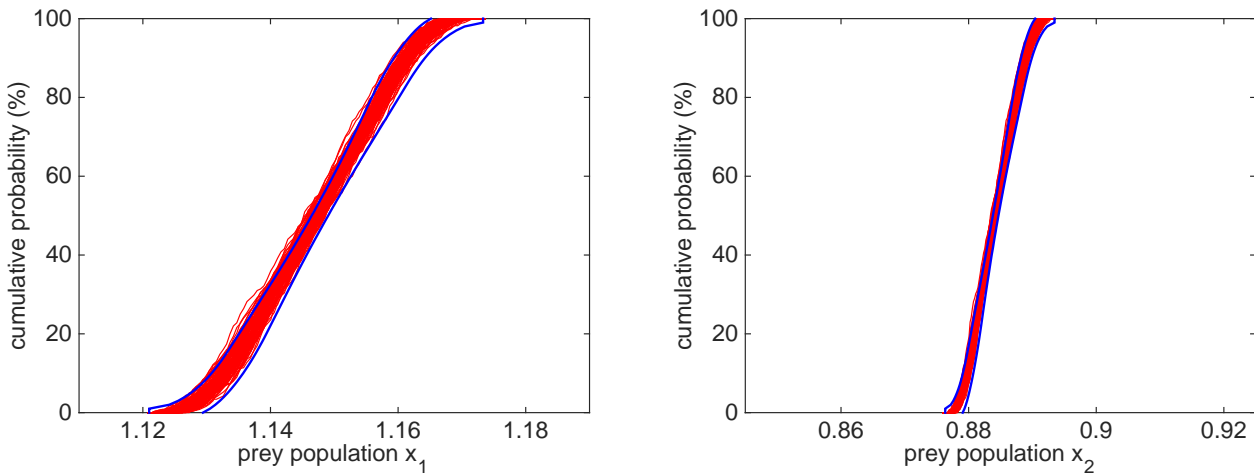


Figure 9: P-boxes (blue) computed from VSPODE Taylor models compared to second-order Monte Carlo simulation (red) for x_1 and x_2 at $t = 10$ for the Lotka-Volterra predator-prey model.

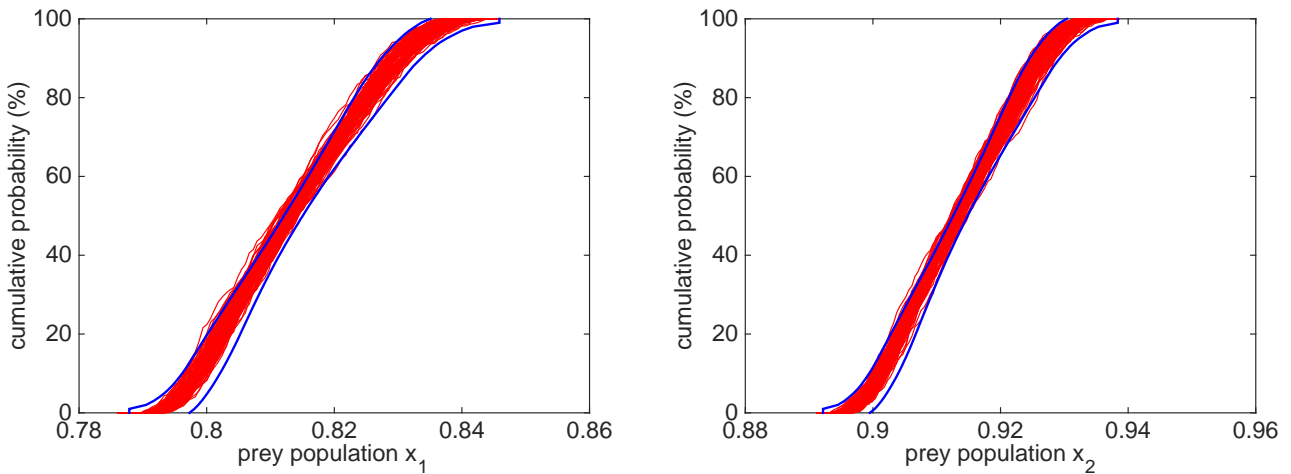


Figure 10: P-boxes (blue) computed from VSPODE Taylor models compared to second-order Monte Carlo simulation (red) for x_1 and x_2 at $t = 20$ for the Lotka-Volterra predator-prey model.

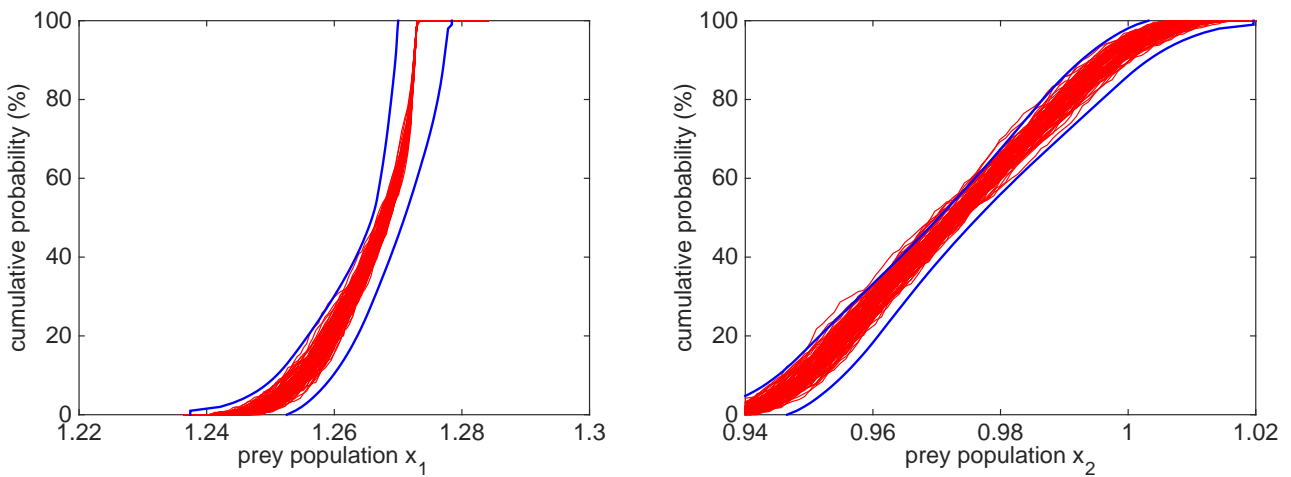


Figure 11: P-boxes (blue) computed from VSPODE Taylor models compared to second-order Monte Carlo simulation (red) for x_1 and x_2 at $t = 25$ for the Lotka-Volterra predator-prey model.

Table 1: Aquatic food web model parameters for varying levels of IL contaminant.

Description	IL concentration			Units	
	0 mg/L	2 mg/L	4 mg/L		
r_C	Intrinsic growth rate constant for C	[0.4, 0.45]	[0.4, 0.45]	[0.4, 0.45]	day ⁻¹
K_C	Carrying capacity for C	5.15×10^{17}	5.20×10^{17}	5.26×10^{17}	indv C
a_{CD}	Loss rate constant for C due to predation by D	[4.00, 4.89] $\times 10^6$	[4.34, 5.44] $\times 10^6$	[4.50, 5.64] $\times 10^6$	(indv C) (indv D) ⁻¹ day ⁻¹
b_C	Half-saturation constant	8.82×10^6	8.82×10^6	8.82×10^6	indv C
a_{CZ}	Loss rate constant for C due to predation by Z	7.47×10^{-11}	7.46×10^{-11}	7.44×10^{-11}	(indv Z) ⁻¹ day ⁻¹
a_{DC}	Growth rate constant for D due to predation on C	0.125	0.0599	0.0599	day ⁻¹
K_D	Carrying capacity for D	3.25×10^{10}	3.25×10^{10}	3.25×10^{10}	indv D
d_D	Intrinsic death rate constant for D	0.0297	0.0470	0.0842	day ⁻¹
a_{ZC}	Growth rate constant for Z due to predation on C	3.78×10^{-23}	3.78×10^{-23}	3.78×10^{-23}	(indv C) ⁻¹ day ⁻¹
d_Z	Intrinsic death rate constant for Z	0.001	0.002	0.003	day ⁻¹
C_0	Initial C population	5.15×10^{16}	5.15×10^{16}	5.15×10^{16}	indv C
D_0	Initial D population	1.25×10^9	1.25×10^9	1.25×10^9	indv D
Z_0	Initial Z population	8.9×10^8	8.9×10^8	8.9×10^8	indv Z

always less than 4×10^{17} . For 2 mg/L contaminant (Fig. 15b), the probability that $C(15) \leq 4 \times 10^{17}$ is bounded by the interval [76, 92]%, and for 4 mg/L (Fig. 15c) by [26, 36]%.

The p-box bounds determined for $C(15)$ are also compared in Fig. 15 to the results of second-order Monte Carlo analysis, with 100 outer loop and 500 inner loop samples. The average computation time for these three cases was 19 seconds for the direct (VSPODE) approach and 870 seconds for the sampling (Monte Carlo) approach. Again, it is seen that the sampling approach is much more expensive computationally, and does not provide rigorous bounds on the state probabilities.

The examples considered here and above all involve two simultaneous uncertain quantities. In another context [8], we have solved a problem with three simultaneous uncertain quantities, and found that the direct approach was again significantly more efficient than sampling. Factors affecting the growth in computation time for the direct method with an increasing number of simultaneous uncertain quantities are discussed in [8]. We expect that problems with a few more simultaneous uncertain quantities could be solved with a feasible computational effort, but have little experience with such problems. Of course, as the number of simultaneous uncertain quantities grows, providing a statistically valid sampling of the corresponding multidimensional space will also be increasingly expensive computationally.

6. Concluding Remarks

Ecological systems modeled using a population ecology approach are best understood if the effects of uncertainty in the model parameters are known. We have

described and demonstrated here a direct approach for rigorously bounding the output trajectories for nonlinear dynamic models in population ecology with uncertain parameters and/or initial conditions, and for rigorously bounding the probability that some specified outcome for a population is achieved. It was shown that this could be done at a computational cost that is significantly less than that required by statistical sampling approaches such as Monte Carlo analysis. We believe that the approach presented here may be useful in several areas of interest in population ecology, including resource management [e.g., 51], invasive species [e.g., 52], and ecotoxicity [e.g., 53].

Another problem of interest in the context of parameter uncertainty is structural sensitivity [e.g., 54, 55]. This refers to the situation in which some small, but finite, change in the model leads to a change in the topological type of the phase portrait. This is often manifested as a change in the structure of one or more of the equilibrium states of the modeled system, e.g., a change in the number of co-existing species. Such structural changes may result from changes in model parameter values or from changes in the form of the model equations. Focusing on structural sensitivity with respect to a parameter change, structural changes occur when the parameter value crosses a bifurcation point. One approach for identifying structural sensitivity is to use sample parameter values from within the interval of uncertainty and run long-time simulations to identify the asymptotic behavior. If the asymptotic behavior is always qualitatively the same, there is no structural sensitivity. The direct approach presented here could be used as an alternative to sampling, but because it determines an envelope

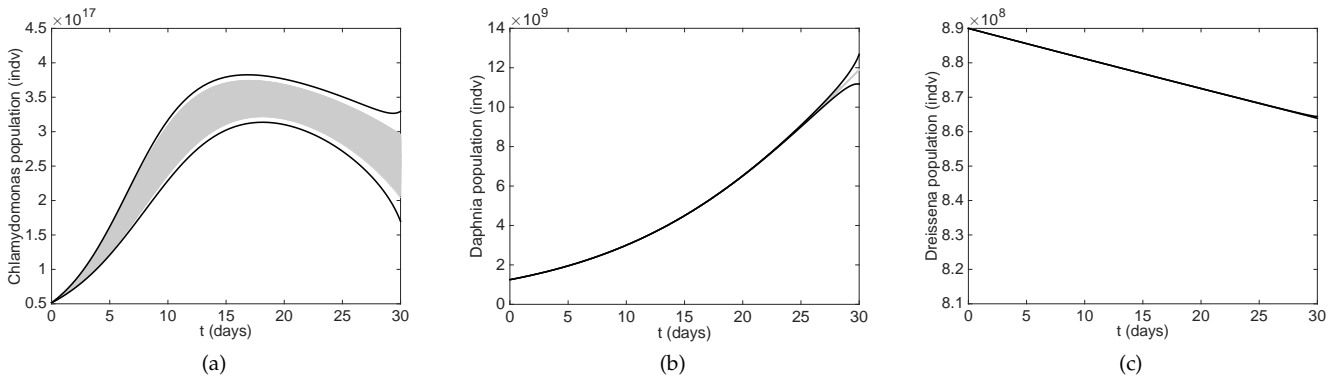


Figure 12: Trajectory bounds for (a) *C. reinhardtii*, (b) *D. magna*, and (c) *D. polymorpha* populations for the aquatic food web model with no contaminant as computed by VSPODE. The results of Monte Carlo simulation are shown in grey.

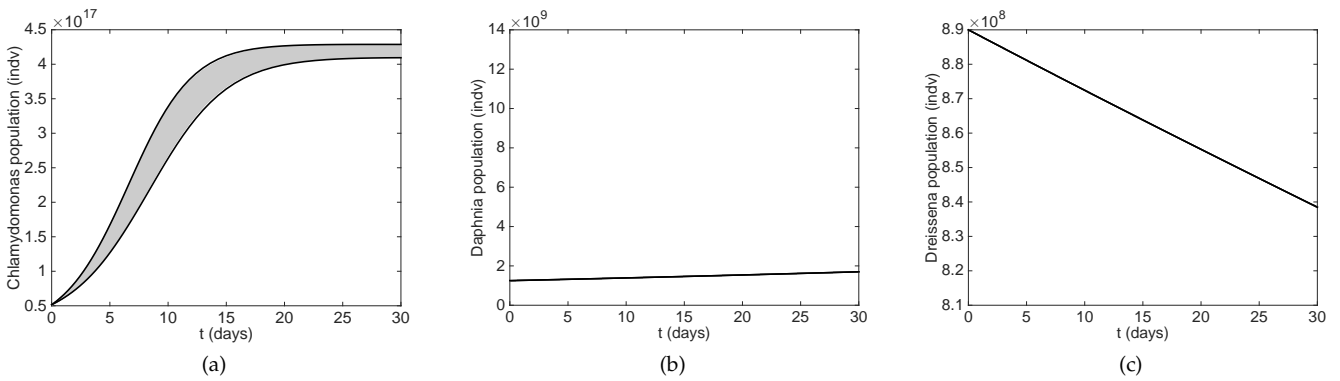


Figure 13: Trajectory bounds for (a) *C. reinhardtii*, (b) *D. magna*, and (c) *D. polymorpha* populations for the aquatic food web model with 2 mg/L contaminant as computed by VSPODE. The results of Monte Carlo simulation are shown in grey.

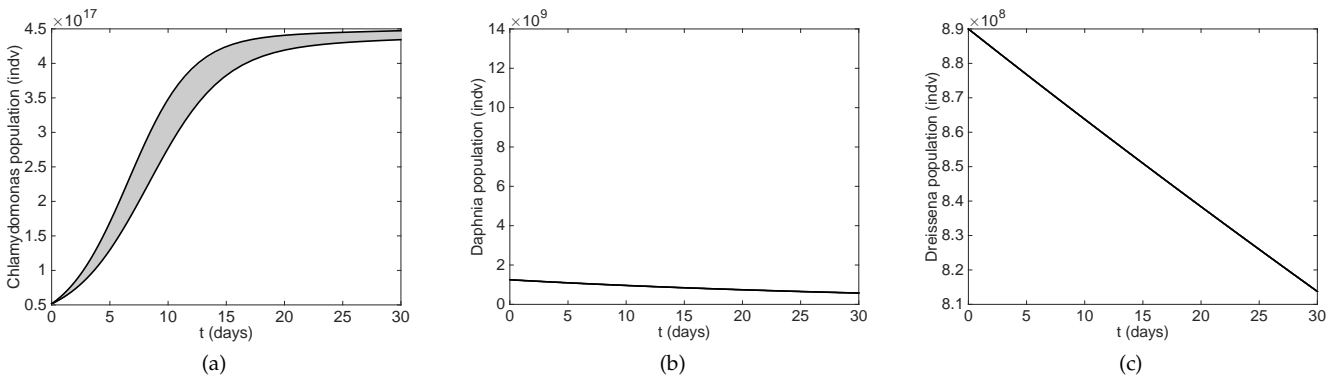
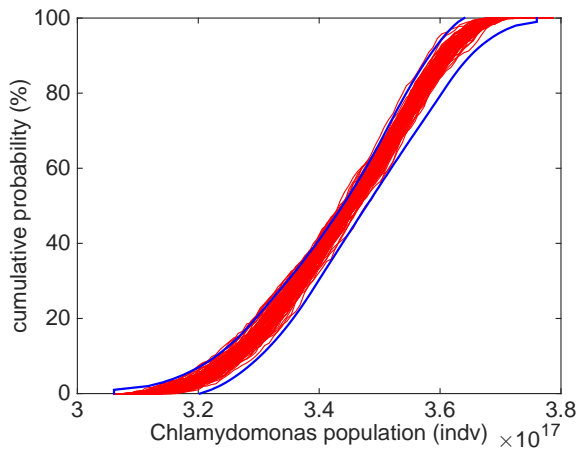
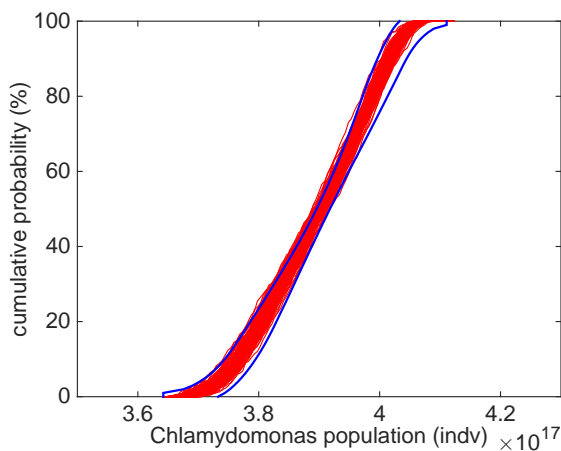


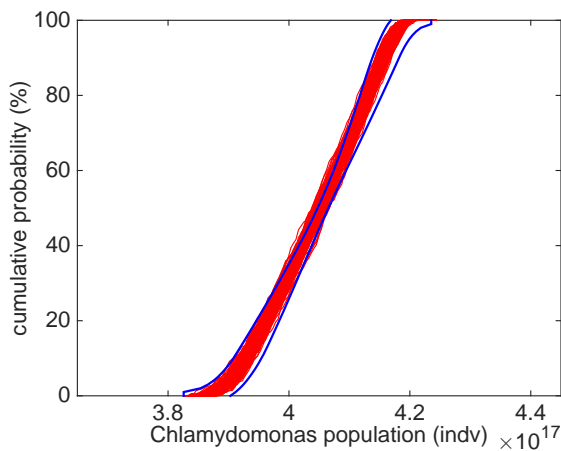
Figure 14: Trajectory bounds for (a) *C. reinhardtii*, (b) *D. magna*, and (c) *D. polymorpha* populations for the aquatic food web model with 4 mg/L contaminant as computed by VSPODE. The results of Monte Carlo simulation are shown in grey.



(a)



(b)



(c)

Figure 15: P-boxes (blue) computed from VSPODE Taylor models compared to second-order Monte Carlo simulation (red) for *C. reinhardtii* populations at 15 days for the aquatic food web model with (a) no contaminant, (b) 2 mg/L contaminant, and (c) 4 mg/L contaminant.

of all possible outcomes, it may not always be possible to clearly identify qualitatively different asymptotic behavior. Another common approach [e.g., 56, 57] is to search directly for the presence of bifurcations; often this is done over a very wide range of parameter values and presented in the form of a bifurcation diagram. While there are various numerical methods used for finding bifurcations [e.g., 58, 59], we have found that for the static bifurcations of equilibrium that correspond to a change in the number of co-existing species (e.g., transcritical, fold) a method based on interval analysis [60] is the most reliable. Given an interval of uncertainty for one or more parameters, this method can be used to easily determine whether or not it contains any appropriate bifurcation points. If there are none, then structural sensitivity with respect to the parameter uncertainty can be ruled out. If a bifurcation is found, and if there are p-boxes for the uncertain parameters, then these could be used directly to determine the probability that a structural change may occur.

References

- [1] M. G. Morgan, M. Henrion, *Uncertainty: A Guide to Dealing with Uncertainty in Quantitative Risk and Policy Analysis*, Cambridge University Press, Cambridge, UK, 1990.
- [2] H. M. Regan, M. Colyvan, M. A. Burgman, A taxonomy and treatment of uncertainty for ecology and conservation biology, *Ecol. Appl.* 12 (2002) 618–628.
- [3] H. M. Regan, H. R. Akçakaya, S. Ferson, K. V. Root, S. Carroll, L. R. Ginzburg, Treatments of uncertainty and variability in ecological risk assessment of single-species populations, *Hum. Ecol. Risk Assess.* 9 (2003) 889–906.
- [4] M. Burgman, *Risks and Decisions for Conservation and Environmental Management*, Cambridge University Press, Cambridge, UK, 2005.
- [5] R. C. Williamson, T. Downs, Probabilistic arithmetic I. Numerical methods for calculating convolutions and dependency bounds, *Int. J. Approx. Reason.* 4 (1990) 89–158.
- [6] S. Ferson, *RAMAS Risk Calc 4.0: Risk Assessment with Uncertain Numbers*, Lewis Press, Boca Raton, FL, 2002.
- [7] F. O. Hoffman, J. S. Hammonds, Propagation of uncertainty in risk assessments: The need to distinguish between uncertainty due to lack of knowledge and uncertainty due to variability, *Risk Anal.* 14 (1994) 707–712.
- [8] J. A. Enszer, Y. Lin, S. Ferson, G. F. Corliss, M. A. Stadtherr, Probability bounds analysis for nonlinear dynamic process models, *AIChE J.* 57 (2011) 404–422.
- [9] E. R. Hansen, G. W. Walster, *Global Optimization Using Interval Analysis*, Marcel Dekker, New York, NY, 2004.
- [10] W. Tucker, *Validated Numerics: A Short Introduction to Rigorous Computations*, Princeton University Press, Princeton, NJ, 2011.
- [11] R. E. Moore, *Interval Analysis*, Prentice-Hall, Englewood Cliffs, NJ, 1966.
- [12] L. Jaulin, M. Kieffer, O. Didrit, É. Walter, *Applied Interval Analysis*, Springer-Verlag, London, 2001.
- [13] R. B. Kearfott, *Rigorous Global Search: Continuous Problems*, Kluwer, Dordrecht, The Netherlands, 1996.
- [14] A. Neumaier, *Interval Methods for Systems of Equations*, Cambridge University Press, Cambridge, UK, 1990.
- [15] R. E. Moore, R. B. Kearfott, M. J. Cloud, *Introduction to Interval Analysis*, SIAM Press, Philadelphia, PA, 2009.
- [16] S. Ferson, L. Ginzburg, R. Akçakaya, Whereof one cannot speak: When input distributions are unknown, Technical Report, Applied Biomathematics, Setauket, NY, 1996. Available at www.ramas.com/whereof.pdf.

- [17] S. Ferson, J. G. Hajagos, Arithmetic with uncertain numbers: Rigorous and (often) best possible answers, *Reliab. Eng. Syst. Safe.* 85 (2004) 135–152.
- [18] D. Berleant, L. Xie, J. Zhang, Statool: A tool for Distribution Envelope determination (DEnv), an interval-based algorithm for arithmetic on random variables, *Reliab. Comput.* 9 (2003) 91–108.
- [19] K. Makino, M. Berz, Remainder differential algebras and their applications, in: M. Berz, C. Bischof, G. Corliss, A. Griewank (Eds.), *Computational Differentiation: Techniques, Applications, and Tools*, SIAM Press, Philadelphia, PA, 1996, pp. 63–74.
- [20] K. Makino, M. Berz, Efficient control of the dependency problem based on Taylor model methods, *Reliab. Comput.* 5 (1999) 3–12.
- [21] K. Makino, M. Berz, Taylor models and other validated functional inclusion methods, *Int. J. Pure Appl. Math.* 4 (2003) 379–456.
- [22] A. Neumaier, Taylor forms – Use and limits, *Reliab. Comput.* 9 (2003) 43–79.
- [23] A. Rauh, E. P. Hofer, E. Auer, ValEncIA-IVP: A comparison with other initial value solvers, in: *Proceedings 12th GAMM - IMACS International Symposium on Scientific Computing, Computer Arithmetic, and Validated Numerics (SCAN 2006)*, 2006, p. 36. DOI: 10.1109/SCAN.2006.47.
- [24] A. B. Singer, P. I. Barton, Bounding the solutions of parameter dependent nonlinear ordinary differential equations, *SIAM J. Sci. Comput.* 27 (2006) 2167–2182.
- [25] A. B. Singer, P. I. Barton, Global optimization with nonlinear ordinary differential equations, *J. Global Optim.* 34 (2006) 159–190.
- [26] N. S. Nedialkov, K. R. Jackson, G. F. Corliss, Validated solutions of initial value problems for ordinary differential equations, *Appl. Math. Comput.* 105 (1999) 21–68.
- [27] M. Neher, K. R. Jackson, N. S. Nedialkov, On Taylor model based integration of ODEs, *SIAM J. Num. Anal.* 45 (2007) 236–262.
- [28] N. S. Nedialkov, K. R. Jackson, J. D. Pryce, An effective high-order interval method for validating existence and uniqueness of the solution of an IVP for an ODE, *Reliab. Comput.* 7 (2001) 449–465.
- [29] N. S. Nedialkov, Interval tools for ODEs and DAEs, in: *Proceedings 12th GAMM - IMACS International Symposium on Scientific Computing, Computer Arithmetic, and Validated Numerics (SCAN 2006)*, IEEE Computer Society, 2006, p. 4. DOI: 10.1109/SCAN.2006.28.
- [30] M. Berz, K. Makino, Verified integration of ODEs and flows using differential algebraic methods on high-order Taylor models, *Reliab. Comput.* 4 (1998) 361–369.
- [31] I. Eble, Über Taylor-Modelle, Ph.D. thesis, Universität Karlsruhe, Karlsruhe, Germany, 2007.
- [32] Y. Lin, M. A. Stadtherr, Validated solutions of initial value problems for parametric ODEs, *Appl. Num. Math.* 57 (2007) 1145–1162.
- [33] A. M. Sahlodin, B. Chachuat, Convex/concave relaxations of parametric ODEs using Taylor models, *Comput. Chem. Eng.* 35 (2011) 844–857.
- [34] A. M. Sahlodin, B. Chachuat, Discretize-then-relax approach for convex/concave relaxations of the solutions of parametric ODEs, *Appl. Num. Math.* 61 (2011) 803–820.
- [35] B. Lambov, Interval arithmetic using SSE-2, in: P. Hertling, C. M. Hoffmann, W. Luther, N. Revol (Eds.), *Reliable Implementation of Real Number Algorithms: Theory and Practice*, Springer, Berlin, 2006, pp. 102–113.
- [36] L. Edelstein-Keshet, *Mathematical Models in Biology*, SIAM, Philadelphia, PA, 2005.
- [37] S. Strogatz, *Nonlinear Dynamics and Chaos: With Applications to Physics, Biology, Chemistry and Engineering*, Perseus Books Group, Cambridge, MA, 2001.
- [38] C. A. Floudas, P. M. Pardalos, C. S. Adjiman, W. R. Esposito, Z. H. Gümüs, S. T. Harding, J. L. Klepeis, C. A. Meyer, C. A. Schwieger, *Handbook of Test Problems in Local and Global Optimization*, Kluwer Academic Publishers, Dordrecht, The Netherlands, 1999.
- [39] J. F. Brennecke, E. J. Maginn, Ionic liquids: Innovative fluids for chemical processing, *AIChE J.* 47 (2001) 2384–2389.
- [40] S. Seo, M. Quiroz-Guzman, M. A. DeSilva, T. B. Lee, Y. Huang, B. F. Goodrich, W. F. Schneider, J. F. Brennecke, Chemically tunable ionic liquids with aprotic heterocyclic anion (AHA) for CO₂ capture, *J. Phys. Chem. B* 118 (2014) 5740–5751.
- [41] S. Seo, L. D. Simoni, M. Ma, M. A. DeSilva, Y. Huang, M. A. Stadtherr, J. F. Brennecke, Phase-change ionic liquids for post-combustion CO₂ capture, *Energy & Fuels* 28 (2014) 5968–5977.
- [42] G. Mozurkewich, L. D. Simoni, M. A. Stadtherr, W. F. Schneider, Performance implications of chemical absorption for the carbon dioxide-cofluid refrigeration cycle, *Int. J. Refrig.* 46 (2014) 196–206.
- [43] D. R. MacFarlane, N. Tachikawa, M. Forsyth, J. M. Pringle, P. C. Howlett, G. D. Elliott, J. H. Davis, M. Watanabe, P. Simon, C. A. Angell, Energy applications of ionic liquids, *Energy Environ. Sci.* 7 (2014) 232–250.
- [44] K. J. Kulacki, D. T. Chaloner, J. H. Larson, D. M. Costello, M. A. Evans-White, K. M. Docherty, R. J. Bernot, M. A. Breuseke, C. F. Kulpa, G. A. Lamberti, Proactive aquatic ecotoxicological assessment of room-temperature ionic liquids, *Curr. Org. Chem.* 15 (2011) 1918–1927.
- [45] T. P. T. Pham, C.-W. Cho, Y.-S. Yun, Environmental fate and toxicity of ionic liquids: A review, *Water Res.* 44 (2010) 352–372.
- [46] M. C. Bubalo, K. Radošević, I. R. Redovniković, J. Halambek, V. G. Srček, A brief overview of the potential environmental hazards of ionic liquids, *Ecotox. Environ. Safe.* 99 (2014) 1–12.
- [47] K. J. Kulacki, Proactive ecological hazard assessment of room-temperature ionic liquids: Aquatic ecotoxicology across scales, Ph.D. thesis, University of Notre Dame, Notre Dame, IN, 2009.
- [48] D. M. Costello, L. Brown, G. Lamberti, Acute toxic effects of ionic liquids on zebra mussel (*Dreissena polymorpha*) survival and feeding, *Green Chem.* 11 (2009) 548–553.
- [49] M. A. Evans-White, G. A. Lamberti, Direct and indirect effects of a potential aquatic contaminant on grazer-algae interactions, *Environ. Toxicol. Chem.* 28 (2009) 418–426.
- [50] K. J. Kulacki, G. Lamberti, Toxicity of imidazolium ionic liquids to freshwater algae, *Green Chem.* 10 (2008) 104–110.
- [51] R. B. Thorpe, W. J. F. Le Quesne, F. Luxford, J. S. Collie, S. Jennings, Evaluation and management implications of uncertainty in a multispecies size-structured model of population and community responses to fishing, *Methods Ecol. Evol.* 6 (2015) 49–58.
- [52] R. A. Erickson, S. M. Presley, L. J. S. Allen, K. R. Long, S. B. Cox, A stage-structured, *Aedes albopictus* population model, *Ecol. Model.* 221 (2010) 1273–1282.
- [53] A. R. Brown, A. M. Riddle, I. J. Winfield, J. M. Fletcher, J. B. James, Predicting the effects of endocrine disrupting chemicals on healthy and disease impacted populations of perch (*perca fluviatilis*), *Ecol. Model.* 189 (2005) 377–395.
- [54] M. W. Adamson, A. Yu. Morozov, Defining and detecting structural sensitivity in biological models: developing a new framework, *J. Math. Biol.* 69 (2014) 1815–1848.
- [55] C. Flora, N. David, G. Mathias, M. Andrew, P. Jean-Christophe, Structural sensitivity of biological models revisited, *J. Theor. Biol.* 283 (2011) 82–91.
- [56] A. Gragnani, O. De Feo, S. Rinaldi, Food chains in the chemostat: Relationships between mean yield and complex dynamics, *Bull. Math. Biol.* 60 (1998) 703–719.
- [57] B. W. Kooi, Numerical bifurcation analysis of ecosystems in a spatially homogeneous environment, *Acta Biotheor.* 51 (2003) 189–222.
- [58] Yu. A. Kuznetsov, *Elements of Applied Bifurcation Theory*, Springer-Verlag, New York, NY, 1998.
- [59] W. J. F. Govaerts, *Numerical Methods for Bifurcations of Dynamical Systems*, SIAM, Philadelphia, PA, 2000.
- [60] C. R. Gwaltney, W. Luo, M. A. Stadtherr, Computation of equilibrium states and bifurcations using interval analysis: Application to food chain models, *Ecol. Model.* 203 (2007) 495–510.